ACS APPLIED BIO MATERIALS
Cite This: ACS Appl. Bio Mater. 2018, 1, 928−935
Article
www.acsabm.org

Acid Susceptible Ultrathin Mesoporous Silica Coated on Layered Double Hydroxide Nanoplates for pH Responsive Cancer Therapy

Wen Cao,[†] Faheem Muhammad,[†] Yuan Cheng,[†] Min Zhou,[†] Qian Wang,[†] Zhangping Lou,[†] Zhe Li,[†] and Hui Wei*[,†,‡]

[†]Department of Biomedical Engineering, College of Engineering and Applied Sciences, Nanjing National Laboratory of Microstructures and [‡]State Key Laboratory of Analytical Chemistry for Life Science and State Key Laboratory of Coordination Chemistry, School of Chemistry and Chemical Engineering, Collaborative Innovation Center of Chemistry for Life Sciences, Nanjing University, Nanjing, Jiangsu 210093, China

Supporting Information

ABSTRACT: Bioresponsive drug delivery systems that can modulate drug release profiles according to different tumor microenvironment are highly desired for improving cancer therapy. In this work, a pH-responsive nanocarrier, layered double hydroxide (LDH) nanoplates coated with ultrathin mesoporous silica layer (LDH@MS), was fabricated with total thickness of around 9 nm. The coating of ultrathin porous silica significantly improved the stability of nanoplates. Moreover, the LDH@MS exhibited pH responsive functionality due to the degradation of silica shell and LDH under moderately acidic pH condition. Notably, the curcumin loaded LDH@MS displayed nearly five-fold greater antitumor efficacy against human breast cancer cells *in vitro* and marked tumor inhibition *in vivo* compared to free curcumin under the same drug dosage, most likely due to high dispersibility of the nanocarrier, as well as responsive and steady release of drug molecules. This study opens new avenues to design safer and more effective drug delivery systems with improved therapeutic outcomes.

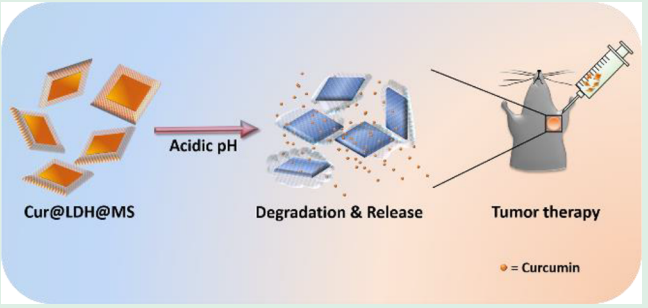

KEYWORDS: *LDH, ultrathin mesoporous silica shell coating, environment stability, biodegradability, pH-responsive tumor therapy*

INTRODUCTION

Chemotherapy, an effective treatment to various cancers, has received considerable therapeutic activities. However, it still has been challenged by poor pharmacokinetics, undesired side effect, and insufficient tumor inhibitory efficacy. To improve the treatment, the drug delivery systems (DDSs), which load molecular drugs onto/into the carriers, have been extensively developed.[1−3] DDSs have exhibited efficient drug loading capacity, improved solubility, enhanced penetration and retention, sustained drug delivery pattern, and customized multiple functionalization.[4] Thanks to the advancement of nanotechnology, a myriad number of nanomaterials have so far been developed and utilized in DDSs.[5−10] Among them, inorganic nanocarriers are preferred over organic ones due to their ease of synthesis, great stability, high loading capacity, and drug release controllability.[11] Representative inorganic nanocarriers are mesoporous silica nanoparticles (MSNs),[12−15] gold nanoparticles,[16] magnetic nanoparticles,[17] carbon nanotubes,[18] black phosphorus,[19] layered double hydroxide (LDH),[20] and so on. Take LDH for instance, it has been explored as a pH responsive drug delivery vehicle for years due to its responsiveness to acidic environments and great biocompatibility. However, the limitations including rapid degradation and burst drug release under acidic conditions hindered its practical usage. Recently, Duan et al. synthesized monolayer LDH nanosheets with high doxorubicin loading content but still fast drug release within hours.[21] On the other hand, in phosphate buffered saline (PBS) or cell culture media, LDH easily agglomerated, which would in turn prevent their *in vivo* applications.[22] Mesoporous silica nanomaterials have been emerged as one of promising DDS materials since 2001.[23] Thereafter, MSNs have been intensively studied due to their distinct properties such as large surface area and pore volume, controllable pore size, morphological homogeneity, feasible surface modification, low systematic toxicity, and superior biocompatibility.[24,25] A few researchers have taken efforts to enhance the stability of LDH by combining LDH with silica materials.[22,26−29] However, these thick silica coating caused the nanoparticles to aggregate to some extent.[26−29] In addition, little work was concentrated to study the biodegradation of silica nanomaterials as silica was considered to be quite stable and inert. Recently, Shi *et al.* synthesized silica nanoparticles doped with manganese and demonstrated tumor-microenvironment sensitive biodegradation and theranostic func-

Received: July 19, 2018
Accepted: August 21, 2018
Published: August 21, 2018

DOI: 10.1021/acsabm.8b00343
ACS Appl. Bio Mater. 2018, 1, 928−935

tions.[30] In this work, we constructed the nanocomposite by coating LDH with ultrathin MS (*i.e.*, LDH@MS), which not only enhanced the stability and pH-responsive drug release functionality of LDH, but also showed biodegradability of MS.

Curcumin, a natural polyphenolic compound, was chosen as the model drug in this work. It has attracted a lot of attention due to its desirable pharmacological efficacies for various diseases[31] including cancer,[32] inflammatory disease,[33] and pulmonary and neurodegenerative disease.[34,35] However, several limitations (such as instability under physiological pH conditions, poor water solubility, and low oral bioavailability) have caused some controversies[36−38] and hampered the potential therapeutic efficacy of curcumin for clinical trials.[39,40] Efforts have been made to improve the bioavailability of curcumin using various strategies including DDSs.[33,41−44] Herein, we selected curcumin molecules as the model drug to study the pH-responsive drug release and antitumor function of LDH@MS (Scheme 1). This system retained the sensitivity of LDH to acidic conditions and the favorable stability of silica. When the model drug curcumin was loaded into LDH@MS, it showed prolonged pH-responsive drug release behavior and enhanced tumor cell killing capacity *in vitro* and tumor inhibition *in vivo* compared with free curcumin.

Scheme 1. Schematic Illustration of pH Responsive Drug Delivery System Based on Mesoporous Silica Coated LDH (LDH@MS) for Cancer Therapy

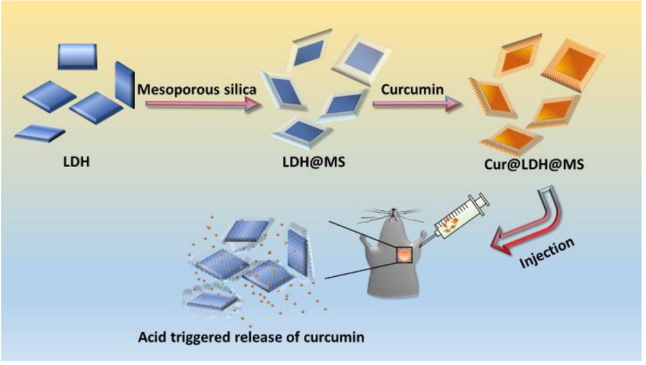

EXPERIMENTAL SECTION

Chemicals and Materials. Cetyltrimethylammonium bromide (CTAB), magnesium chloride ($MgCl_2·6H_2O$), aluminum chloride ($AlCl_3·6H_2O$), ammonia solution 25% (wt/v), sodium hydroxide (NaOH), and curcumin were purchased from Sinopharm Chemical Reagent Co., Ltd. Tetraethyl orthosilicate (TEOS) and (3-aminopropyl) triethoxysilane (APTES) were purchased from Aladdin Chemical Reagent Co., Ltd. All chemicals were used as received without further purifications. All aqueous solutions were prepared with deionized water (18.2 MΩ cm, Millipore).

Instruments. Scanning electron microscopy (SEM) images were obtained by using a ZEISS ultra 55 scan electron microscope. Transmission electron microscopy (TEM) images were obtained by using JEM-200CX transmission electron microscopy. Power X-ray diffraction (XRD) was recorded at room temperature on a XTRA X-ray diffraction with a scan rate of 5° min^{-1}. The inductively coupled plasma mass spectrometry (ICP-MS) data were collected on ELAN 9000. The X-ray photoelectron spectroscopy (XPS) results were obtained by using PHI 5000 VersaProbe. Dynamic lighting scattering (DLS) and zeta potential distribution were measured on Nanosizer ZS90 (Malvern) using deionized water as dispersants. UV−visible absorption spectra were collected on a UV−visible spectrophotometer (TU-1900, Beijing Purkinje General Instrument Co. Ltd., China). Atomic force microscope (AFM) images were obtained by using Bruker MultiMode 8. Surface area data were collected on Micromeritics ASAP 2020 surface area and porosity analyzer after pretreating at 120 °C for 12 h and calculated with the Brunauer−Emmett−Teller (BET) method. Fourier transform infrared (FTIR) spectra were obtained with NEXUS870 Fourier transform infrared spectrometer. Photoluminescence spectra were measured on a Hitachi F-4600 spectrometer. Confocal laser scanning microscopy (CLSM) data were obtained using Olympus IX-83.

Synthesis of Mg−Al LDH Nanoplates. LDH nanoplates were synthesized using a previously reported method.[29] In brief, 40.0 mL of NaOH solution (0.15 M) was added into 10.0 mL of solution containing 3.0 mmol of $MgCl_2$ and 1.0 mmol of $AlCl_3$ under vigorous magnetic stirring. The obtained precipitate was separated by centrifugation (5000 rpm, 1 min) and washed twice with water. The precipitate was redispersed in 40.0 mL of water, sealed into a Teflon-lined stainless steel autoclave, and heated at 110 °C for 5 h. The products (with solution) were collected and ready for silica coating.

Synthesis of LDH@MS. Briefly, 0.6 g of CTAB (1.6 mmol) was dissolved in the mixture of 140.0 mL of water and 120.0 mL of ethanol. Then 1.0 mL of ammonia solution (25 wt %/v) and 20.0 mL suspension of as-prepared LDH nanoplates were added and magnetically stirred for 10 min. Afterward, 200.0 μL of TEOS was added under vigorous stirring. After another 30 min, the product was collected by centrifugation (10 000 rpm, 2 min) and washed twice with ethanol.

Functionalization of LDH@MS with $-NH_2$ Group. To functionalize LDH@MS with $-NH_2$ group, the LDH@MS product was redispersed with 50.0 mL of ethanol. Then 100.0 μL of APTES was added. The resultant suspension was heated at 80 °C and refluxed for 3 h. Then LDH@MS-NH_2 was washed twice with ethanol and dispersed with 50.0 mL of ethanol. To remove CTAB, 2.0 g of NH_4NO_3 was added to the solution and refluxed at 60 °C for 1 h. After that, the product was washed twice with water and dried at 40 °C.

Synthesis of LDH@MS-NH_2−FITC. LDH@MS-NH_2 (20.0 mg) was dispersed in 3.0 mL of water with FITC (15.0 mg) and stirred for 2 h in the darkness. The product was collected by centrifugation (10 000 rpm, 5 min), washed three times with ethanol, and kept at 4 °C in the darkness.

Drug Loading and *in Vitro* Release. Fifty milligrams of LDH@MS-NH_2 was added in DMSO solution of 10.0 mg of curcumin (5.0 mg/mL) and stirred for 3 h. After centrifugation (14 800 rpm, 5 min), the sample was redispersed in 1.0 mL of water and stirred for 2 h. Finally, the product (Cur@LDH@MS-NH_2) was washed twice with water for further characterization.

To determine the loading quantity of curcumin, 2.0 mg of Cur@LDH@MS-NH_2 was immersed into a pH = 2.0 NaAc-HAc solution and sonicated for 30 min. The completely released curcumin (i.e., the loaded quantity of curcumin) was determined by measuring the absorbance at 425 nm.

To study the drug release profile, 2.0 mg of Cur@LDH@MS-NH_2 was dispersed into 1.0 mL of pH = 7.4 phosphate-buffered saline buffer and pH = 5.0 NaAc-HAc buffer, respectively. Then they were dialyzed (MWCO = 8000) against 5.0 mL of corresponding buffer and ethanol mixed solution (volume ratio = 3:2) at room temperature. The released curcumin in the buffer was collected at predetermined times and quantitated by UV−visible spectroscopy at 425 nm.

Cell Viability and Cellular Uptake. Human breast cancer cell line (MCF-7) was cultured in high glucose DMEM culture medium containing 10% fetal bovine serum (FBS) and 1% penicillin−streptomycin (10 000 U/mL) under the atmosphere of 5% CO_2 at 37 °C. MCF-7 cells were seeded in 96-well plates with a density of 8.0×10^3 cells per well and incubated for 24 h. Then free curcumin, LDH@MS-NH_2, and Cur@LDH@MS-NH_2 with different concentrations were added, respectively. After 72 h, the cells of all groups were washed with PBS three times and the cell viability was

DOI: 10.1021/acsabm.8b00343
ACS Appl. Bio Mater. 2018, 1, 928−935

determined using 3-(4, 5-dimethyl-2-thiazolyl)-2, 5-diphenyl-2-H-tetrazolium bromide (MTT) assay.

For confocal imaging study, MCF-7 cells were seeded in 24-well plates and incubated for 24 h. Then the cells were treated with LDH@MS-NH_2−FITC (30 μg/mL) and Cur@LDH@MS-NH_2 (30 μg/mL), respectively, and observed at different predetermined time. The nuclei were stained with Hoechst for cellular uptake observation. The excitation wavelengths of LDH@MS-NH_2−FITC and Cur@LDH@MS-NH_2 were 488 and 405 nm, respectively, and the emission wavelength for both was 520 nm.

Antitumor Effects of Cur@LDH@MS-NH_2. All the animal experiments were reviewed and approved by the Committee for Experimental Animals Welfare and Ethics of Nanjing Drum Tower Hospital, the Affiliated Hospital of Nanjing University Medical School. Murine H22 cells (1.0×10^6) were subcutaneously injected into the right limb armpits of each of 40 ICR male mice. The mice were kept for 7 d with free access to food and water and randomly divided into four groups (10 mice per group). When the tumor volume reached 60 mm^3 on average, 200.0 μL of saline, LDH@MS-NH_2, free curcumin, and Cur@LDH@MS-NH_2 solution at a curcumin dose of 10 mg/kg body weight were administrated into tumor area, respectively. The day was designated as Day 1. The tumor volume was measured every other day using calipers and calculated following the equation:

$$\text{Volume} = (\text{length} \times \text{width}^2)/2$$

Histological Study. On the 30th day after administration, the mice of all group were sacrificed and the tumor tissues from each group were collected and rinsed with water, and then fixed in 10% neutral buffered formalin. The tumors were processed routinely, dried and embedded into paraffin, sectioned at a thickness of 4 mm, stained with hematoxylin and eosin (HE), examined, and photographed by an optical microscopy.

RESULTS AND DISCUSSION

Preparation and Characterization of LDH@MS-NH_2. As shown in Scheme 1, to realize the pH triggered drug delivery nanosystem, we synthesized MS coated LDH nanoplates using two steps: (1) preparation of monodispersed LDH nanoplates; (2) ultrathin MS coating on the nanoplates to form LDH@MS.

The parent LDH nanoplates had good dispersibility as shown in Figures 1a and S1a. However, the hydroxide of the LDH is quite sensitive to acidic conditions and easily agglomerates in PBS (as shown in Figure S5), and surface coating is therefore necessary to improve the stability of LDH nanoplates. Mesoporous silica is a sort of physicochemically stable and inert materials with low cytotoxicity, so uniform mesoporous silica coating can enhance the structural stability of LDH nanoplates and maintain the biocompatibility of LDH. Moreover, water dispersibility is of paramount importance in view of nanodrug carrier because it helps enhance the blood circulation and target site penetration of the nanocarriers as well as drug release content.[4] Therefore, we coated the LDH with a proper silica layer to endow LDH with greater water dispersibility and better stability. For high-quality mesoporous silica coating, we optimized the ratio of LDH and TEOS by varying the amount of TEOS. As shown in Figures S1−S3, with the increase of TEOS from 200 to 800 μL, the LDH@MS became less dispersive. Therefore, the LDH@MS (200 μL TEOS) with good dispersibility was chosen for further study.

The coating of LDH nanoplates with MS was analyzed through electron microscopy (Figure 1b). The size of LDH@MS was around 94.3 ± 26.7 nm with a relatively narrow size distribution and the particles were well separated. To improve the stability in aqueous solution and provide drug molecules

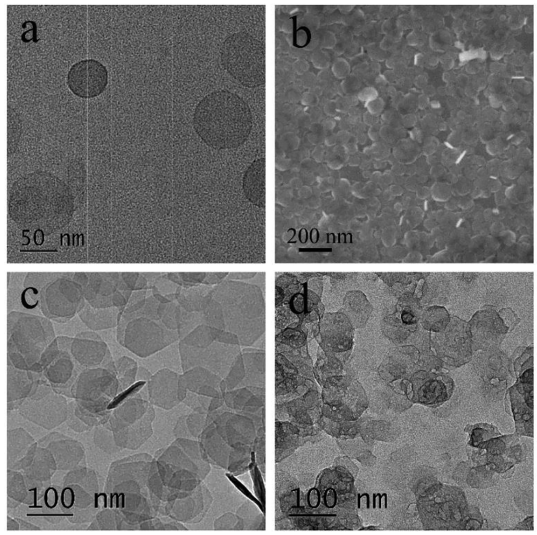

Figure 1. (a) TEM image of LDH; (b) SEM image of LDH@MS; TEM images of (c) LDH@MS-NH_2 and (d) LDH@MS-NH_2 exposure to pH 5.0.

anchoring sites to LDH@MS, the surface of LDH@MS nanoplates was further functionalized with amine moiety (APTES). TEM images provided more detailed information about the thickness and mesoporous structure of silica coating. Figure 1c indicated the well-defined, uniform and highly dispersed LDH@MS-NH_2. The size of LDH@MS-NH_2 was 95.1 ± 26.5 nm, which was comparable with parent LDH (88.6 ± 26.5 nm). To characterize the thickness of the silica shell, AFM imaging was used. As shown in Figure S4, the thickness of LDH and LDH@MS-NH_2 was about 5 and 9 nm, respectively. The thickness of silica shell was then calculated to be around 2 nm. Importantly, on contrary to previous reports,[26−29] no aggregation could be observed, indicating the high stability and dispersity of LDH@MS-NH_2.

DLS size, polydispersity index (PDI), surface charge, and BET surface area of LDH nanoplates, LDH@MS and LDH@MS-NH_2, are summarized in Table S1. The DLS size difference between LDH nanoplates and LDH@MS further demonstrated that the coating of silica layer was successful. The amino groups indeed improved the dispersibility of LDH@MS and brought the particle size back from 360.4 to 181.6 nm due to the inhibition of particle aggregations. Moreover, the lowest PDI among these three samples indicated the final LDH@MS-NH_2 is well dispersive. The surface area of parent LDH was about 23 m^2/g, while it grew to 99 m^2/g after mesoporous silica layer coating. The surface area difference indicated that MS coating was distinct, and the larger surface of the carrier provided more contact and storage area for the model drug. To further demonstrate the silica coating and the $-NH_2$ group modification, XPS analysis was carried out (Figures S6 and S7). The appearance of Si 2p peak (Figure 2a) indicated the silica layer coating and the existence of N 1s peak (Figure 2b) convincingly proved the presence of $-NH_2$ group. From XRD results (Figure 2c), it could be seen that the crystalline nature of LDH nanoplates was consistent with previous reports.[45] After MS coating, the intensity of LDH peaks was slightly lowered, while the crystal structure of LDH remained intact, indicating the silica coating did not influence the structure of LDH.

DOI: 10.1021/acsabm.8b00343
ACS Appl. Bio Mater. 2018, 1, 928−935

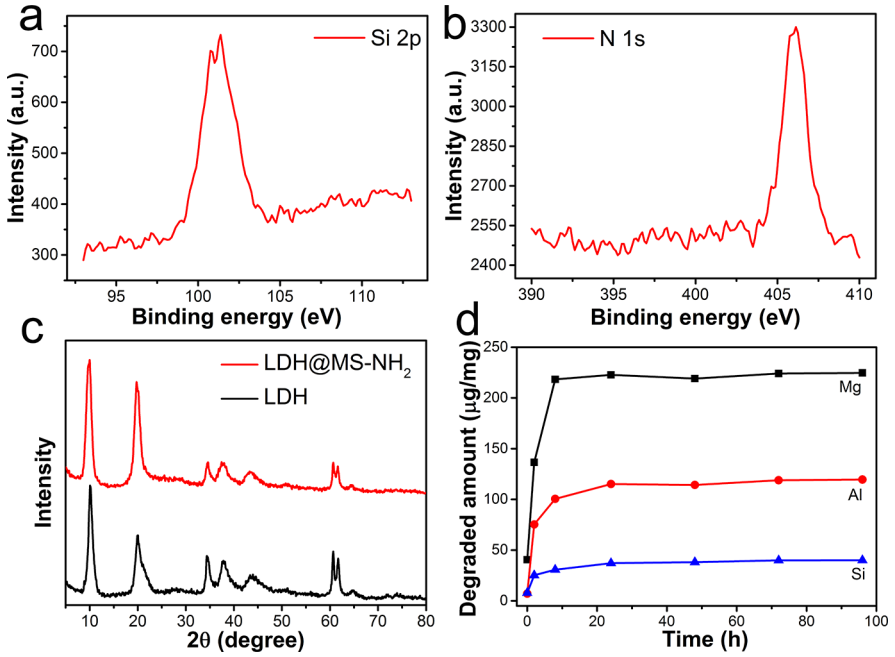

Figure 2. XPS spectrum of (a) Si 2p and (b) N 1s of LDH@MS-NH_2; (c) powder XRD patterns of LDH and LDH@MS-NH_2; (d) time-dependent degraded amounts of Mg, Al, and Si elements after exposing to pH 5.0 solution.

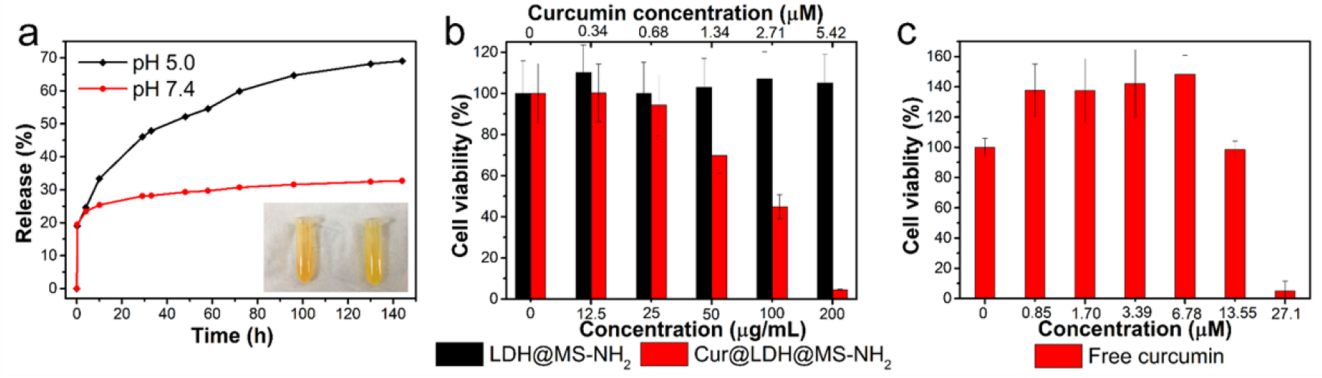

Figure 3. (a) Curcumin release profile from LDH@MS-NH_2 at pH 7.4 and 5.0. Inset: digital picture of Cur@LDH@MS-NH_2 at pH = 7.4 (left) and pH = 5.0 (right). (b) Cell viability data of LDH@MS-NH_2 and Cur@LDH@MS-NH_2. (c) Cell viability data of free curcumin against MCF-7 cancer cells.

Mesoporous silica has been considered quite stable in various environments, but in this study we found the slow degradation of the structure of silica shell over the period of time. Upon exposing the LDH@MS-NH_2 to mildly acidic solution, the integrity of core−shell structure was progressively compromised. The morphology change of LDH@MS-NH_2 was accompanied by obvious destruction of materials' structure (Figure 1d).

To definitely study acid sensitive behavior of LDH@MS-NH_2, the material was immersed into mild acidic solution (pH = 5.0) and the ICP-MS analysis of supernatants was carried out at predetermined time. As shown in Figure 2d, magnesium hydroxide component of LDH was found the most sensitive to the acid solution and showed the abrupt and earliest degradation within 8 h. Besides, the degradation of Si was also observed over time, which was quite evident in terms of the stable nature of silica. Magnesium hydroxide, aluminum hydroxide, and silica showed the capacity of degradation when exposed to mild acidic environment without exception. By exploiting this interesting biodegradability behavior, the LDH@MS-NH_2 was utilized as a pH-responsive antitumor drug carrier because of the mildly acidic microenvironment of tumor tissues.

Drug Loading and *in Vitro* Release. To study the drug delivery functionality, curcumin was loaded into LDH@MS-NH_2 to form Cur@LDH@MS-NH_2. As shown in Scheme 1, curcumin can be loaded by two different paths. The first one was based on the strong chelation between the metal ions of LDH and curcumin, which has a diketone moiety and can be transformed to a keto−enol tautomeric form.[46] The peak of 418.48 cm^{-1} in the FTIR spectrum of Cur@LDH@MS-NH_2 indicated the interaction between the metal ion and O atom of curcumin (Figure S8).[47] LDH@MS-NH_2 loaded with curcumin showed strong a UV−visible absorption (Figure S9), further demonstrating the formation of metal complex.[46] The other one was that the larger surface area of MS provided further space for curcumin loading. The loading amount was calculated to be 27.1 μmol/g according to UV−visible absorption spectroscopic measurement. Notably, the dispersibility of the nanocomposite exhibited no obvious changes after

DOI: 10.1021/acsabm.8b00343
ACS Appl. Bio Mater. 2018, 1, 928−935

curcumin loading (digital picture in Figure 3a inset). Curcumin release profiles were studied in different buffer solutions of pH 5.0 and 7.4 (Figure 3a). A pH responsive release manner was observed due to the degradation of both LDH and silica coating at acidic condition. To compare with the release behavior of LDH, we also loaded curcumin in parent LDH and studied the curcumin release profile (Figure S10). The complete and burst drug release was achieved (within 2 h) in case of LDH, while comparatively slow and steady release behavior was observed with LDH@MS-NH_2. The initial release amount (about 25%) at pH 5.0 and 7.4 for LDH@MS was almost the same in the first 5 h, which implied that drug release was most likely resulted from mesoporous surface of silica shell. However, the release at pH 5.0 was gradually increased to 70% until 140 h, which was probably due to the degradation of core−shell structure, while in the case of pH 7.4 the total release amount was found to be about 30% over the same duration. Taken together, silica coating not only improved the stability of LDH, but also achieved desirable controlled drug release profile.

To evaluate the biocompatibility of LDH@MS-NH_2, different concentrations of drug loaded and empty nanoplates were tested against human breast cancer cells (MCF-7). As shown in Figure 3b, LDH@MS-NH_2 itself exhibited no obvious influence to cell viability even at a concentration of 200 μg/mL, demonstrating the excellent biocompatibility. The efficiency difference between free curcumin and Cur@LDH@MS-NH_2 was evaluated to demonstrate the advantage of this drug delivery system. For free curcumin, the lethal dosage was found to be about 27.1 μM (Figure 3c), while a much lower lethal dosage value (5.42 μM) was observed for Cur@LDH@MS-NH_2. Besides, free curcumin showed the auxo-action of cancer cell growth at lower concentrations ($\leq$6.78 μM), which was not observed with Cur@LDH@MS-NH_2.[48] These results demonstrated Cur@LDH@MS-NH_2 enhanced the tumor cell killing capacity of curcumin.

LDH@MS-NH_2 was labeled with FITC and observed by confocal laser scan microscopy to study the cellular uptake behavior. As shown in Figure 4, LDH@MS-NH_2−FITC were internalized within a short period of incubation as proved by the intracellular appearance of green fluorescence. Furthermore, the overlay of bright field and FITC fluorescence images also strongly indicated the intracellular localization of nanocarriers. This was the evidence of the remarkable cellular uptake efficacy of nanocarriers, which contributed to the tumor cell killing capacity of this nanosystem.

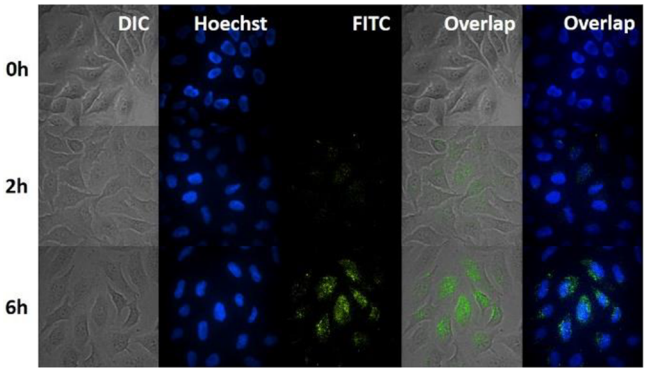

Figure 4. CLSM images of MCF-7 cells incubated for different time with a culture medium with FITC labeled LDH@MS-NH_2. For each channel, the images from left to right show differential interference contrast (DIC) images, cell nuclei stained by Hoechst (blue), FITC fluorescence in cells (green), and overlays of the images. The magnification is 40×.

Confocal microscopy was similarly used to determine the cellular uptake and curcumin release by incubating the MCF-7 cells with a definite amount of Cur@LDH@MS-NH_2. The fluorescence of curcumin was quenched when it was loaded in LDH@MS-NH_2 (Figure S11). Following the incubation of curcumin loaded sample, more intense greenish luminescence was observed in the cytoplasmic regions with passage of time, indicating the cellular uptake of drug loaded nanoparticles (Figure 5). On the basis of the cellular uptake of FITC labeled nanocarriers within 6 h, it was easy to find out that the curcumin release behavior was slow but steady. This result was in accordance with Figure 3a and provided further evidence of the advantage of LDH@MS-NH_2 nanocarrier.

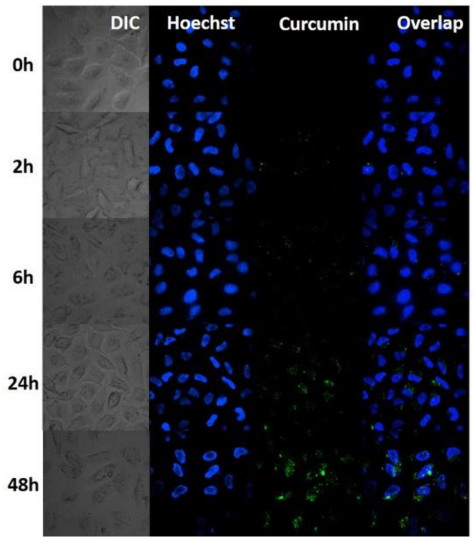

Figure 5. *In vitro* drug release. CLSM micrographs of MCF-7 cells treated with curcumin loaded LDH@MS-NH_2. For each channel, the images from left to right show differential interference contrast (DIC) images, cell nuclei stained by Hoechst (blue), curcumin fluorescence in cells (green), and overlays of the images. The magnification is 40×.

***In Vivo* Antitumor Effect.** More importantly, to evaluate the antitumor effect of Cur@LDH@MS-NH_2, the *in vivo* tumor inhibition experiments have been conducted by using H22 tumor bearing mice. As shown in Figure 6a, compared with saline and empty LDH@MS-NH_2, free curcumin displayed 50% tumor inhibition after 15 days, while Cur@LDH@MS-MH_2 showed better efficacy and tumor inhibition percentage reached 75%. The body weight of the mice in each group was monitored to evaluate the biosafety of the material and summarized in Figure 6b. The body weight of empty LDH@MS-NH_2 treated group increased in the same pace with the control group of saline, indicating that empty LDH@MS-NH_2 exhibited no obvious toxicity *in vivo*.

The images of HE stained tumor sections of tested ICR mice after 30 days postinjection are shown in Figure 6c−f, which distinctly showed the tumor cells from the groups treated with saline and empty LDH@MS-NH_2. On the other hand, the degree of pathological cytokinesis in the tumor was lowered and coagulation necrosis was enhanced in the group treated with free curcumin and Cur@LDH@MS-NH_2 due to the

DOI: 10.1021/acsabm.8b00343
ACS Appl. Bio Mater. 2018, 1, 928−935

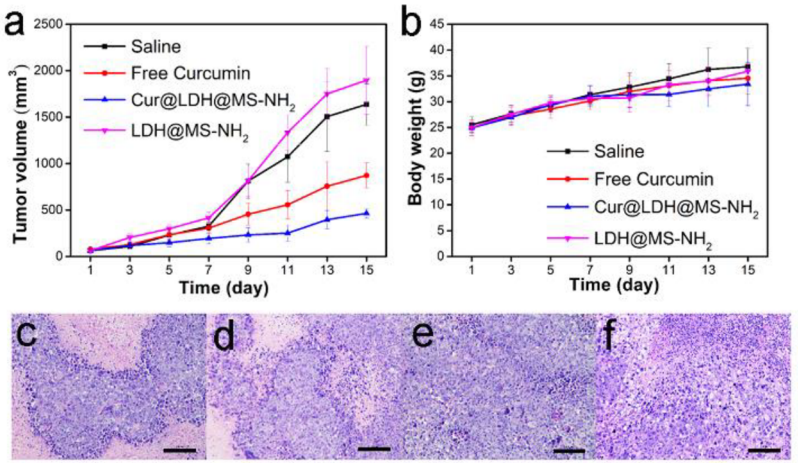

Figure 6. *In vivo* antitumor effect. (a) Tumor growth and (b) weight change profiles of H22 cancer cells bearing mice after different treatments. The injection dose of curcumin was 10 mg/kg. HE stained tumor section 30 d after injecting (c) saline, (d) free curcumin, (e) empty LDH@MS-NH_2, and (f) Cur@LDH@MS-NH_2, respectively. The scale bar is 100 μm.

antitumor effect of curcumin. All the results above demonstrated LDH@MS-NH_2 could be served as an effective antitumor drug carrier and showed great biocompatibility and capacity of drug releasing within tumor area.

CONCLUSIONS

In summary, we fabricated a smart drug delivery system, which is composed of 2D LDH nanoplates and ultrathin MS with total thickness of about 9 nm. We demonstrated that the MS coating on LDH not only remarkably improved the stability of LDH, but also provided better pH responsive functionality. The acid responsive degradation of porous silica shell and LDH core was exploited to develop a pH responsive drug delivery system. When curcumin as a model drug was loaded within LDH@MS-NH_2 nanocarrier, it exhibited an improved performance with a five-fold higher tumor cell killing efficacy against MCF-7 cells *in vitro* when compared with free curcumin with the same dosage. Furthermore, Cur@LDH@MS-NH_2 also displayed enhanced *in vivo* antitumor effect against liver cancer model (H22). The developed LDH@MS was endowed with advantages of both LDH and MS and provided a new strategy for long-term controlled drug release and great biocompatibility and biodegradation compared to traditional LDH and MS, respectively.

ASSOCIATED CONTENT

Supporting Information

The Supporting Information is available free of charge on the ACS Publications website at DOI: 10.1021/acsabm.8b00343.

Extra figures with associated discussion; tables (DOCX)

AUTHOR INFORMATION

Corresponding Author

*E-mail: weihui@nju.edu.cn. Phone: +86-25-83593272. Fax: +86-25-83594648.

ORCID

Zhe Li: 0000-0002-2755-2409

Hui Wei: 0000-0003-0870-7142

Notes

The authors declare no competing financial interest.

ACKNOWLEDGMENTS

This work was supported by National Natural Science Foundation of China (21722503 and 21874067), 973 Program (2015CB659400), PAPD program, Shuangchuang Program of Jiangsu Province, Open Funds of the State Key Laboratory of Analytical Chemistry for Life Science (SKLACLS1704), Open Funds of the State Key Laboratory of Coordination Chemistry (SKLCC1819), Fundamental Research Funds for the Central Universities (021314380103 and 021314380119), and Thousand Talents Program for Young Researchers.

REFERENCES

(1) Frandsen, J. L.; Ghandehari, H. Recombinant Protein-Based Polymers for Advanced Drug Delivery. *Chem. Soc. Rev.* **2012**, *41* (7), 2696−2706.

(2) Mura, S.; Nicolas, J.; Couvreur, P. Stimuli-Responsive Nanocarriers for Drug Delivery. *Nat. Mater.* **2013**, *12* (11), 991−1003.

(3) Hu, Q.; Katti, P. S.; Gu, Z. Enzyme-Responsive Nanomaterials for Controlled Drug Delivery. *Nanoscale* **2014**, *6* (21), 12273−12286.

(4) Shi, J.; Kantoff, P. W.; Wooster, R.; Farokhzad, O. C. Cancer Nanomedicine: Progress, Challenges and Opportunities. *Nat. Rev. Cancer* **2017**, *17* (1), 20−37.

(5) Pan, D.; Caruthers, S. D.; Hu, G.; Senpan, A.; Scott, M. J.; Gaffney, P. J.; Wickline, S. A.; Lanza, G. M. Ligand-Directed Nanobialys as Theranostic Agent for Drug Delivery and Manganese-Based Magnetic Resonance Imaging of Vascular Targets. *J. Am. Chem. Soc.* **2008**, *130* (29), 9186−9187.

(6) Liu, P.; Shi, B. H.; Yue, C. X.; Gao, G. H.; Li, P.; Yi, H. Q.; Li, M. X.; Wang, B.; Ma, Y. F.; Cai, L. T. Dextran-Based Redox-Responsive Doxorubicin Prodrug Micelles for Overcoming Multidrug Resistance. *Polym. Chem.* **2013**, *4* (24), 5793−5799.

(7) Du, J.; Lane, L. A.; Nie, S. Stimuli-Responsive Nanoparticles for Targeting the Tumor Microenvironment. *J. Controlled Release* **2015**, *219*, 205−214.

(8) Lei, B.; Wang, M.; Jiang, Z.; Qi, W.; Su, R.; He, Z. Constructing Redox-Responsive Metal-Organic Framework Nanocarriers for Anticancer Drug Delivery. *ACS Appl. Mater. Interfaces* **2018**, *10* (19), 16698−16706.

(9) Cho, H. Y.; Lee, T.; Yoon, J.; Han, Z.; Rabie, H.; Lee, K. B.; Su, W. W.; Choi, J. W. Magnetic Oleosome as a Functional Lipophilic Drug Carrier for Cancer Therapy. *ACS Appl. Mater. Interfaces* **2018**, *10* (11), 9301−9309.

(10) Liu, Y.; Shao, C.; Bian, F.; Yu, Y.; Wang, H.; Zhao, Y. Egg Components Composited Inverse Opal Particles for Synergistic Drug Delivery. *ACS Appl. Mater. Interfaces* **2018**, *10* (20), 17058−17064.

(11) Liong, M.; Lu, J.; Kovochich, M.; Xia, T.; Ruehm, S. G.; Nel, A. E.; Tamanoi, F.; Zink, J. I. Multifunctional Inorganic Nanoparticles for Imaging, Targeting, and Drug Delivery. *ACS Nano* **2008**, *2* (5), 889−896.
(12) Chen, H.; Zhen, Z.; Tang, W.; Todd, T.; Chuang, Y.-J.; Wang, L.; Pan, Z.; Xie, J. Label-Free Luminescent Mesoporous Silica Nanoparticles for Imaging and Drug Delivery. *Theranostics* **2013**, *3* (9), 650−657.
(13) Chen, C.; Geng, J.; Pu, F.; Yang, X.; Ren, J.; Qu, X. Polyvalent Nucleic Acid/Mesoporous Silica Nanoparticle Conjugates: Dual Stimuli-Responsive Vehicles for Intracellular Drug Delivery. *Angew. Chem., Int. Ed.* **2011**, *50* (4), 882−886.
(14) Muhammad, F.; Guo, M.; Qi, W.; Sun, F.; Wang, A.; Guo, Y.; Zhu, G. pH-Triggered Controlled Drug Release from Mesoporous Silica Nanoparticles via Intracelluar Dissolution of ZnO Nanolids. *J. Am. Chem. Soc.* **2011**, *133* (23), 8778−8781.
(15) Guo, R.; Li, L.-L.; Zhao, W.-H.; Chen, Y.-X.; Wang, X.-Z.; Fang, C.-J.; Feng, W.; Zhang, T.-L.; Ma, X.; Lu, M.; Peng, S.-Q.; Yan, C.-H. The Intracellular Controlled Release from Bioresponsive Mesoporous Silica with Folate as Both Targeting and Capping Agent. *Nanoscale* **2012**, *4* (11), 3577−3583.
(16) Pissuwan, D.; Niidome, T.; Cortie, M. B. The Forthcoming Applications of Gold Nanoparticles in Drug and Gene Delivery Systems. *J. Controlled Release* **2011**, *149* (1), 65−71.
(17) Reddy, L. H.; Arias, J. L.; Nicolas, J.; Couvreur, P. Magnetic Nanoparticles: Design and Characterization, Toxicity and Biocompatibility, Pharmaceutical and Biomedical Applications. *Chem. Rev.* **2012**, *112* (11), 5818−5878.
(18) Liu, Z.; Chen, K.; Davis, C.; Sherlock, S.; Cao, Q. Z.; Chen, X. Y.; Dai, H. J. Drug Delivery with Carbon Nanotubes for *In Vivo* Cancer Treatment. *Cancer Res.* **2008**, *68* (16), 6652−6660.
(19) Tao, W.; Zhu, X.; Yu, X.; Zeng, X.; Xiao, Q.; Zhang, X.; Ji, X.; Wang, X.; Shi, J.; Zhang, H.; Mei, L. Black Phosphorus Nanosheets as a Robust Delivery Platform for Cancer Theranostics. *Adv. Mater.* **2017**, *29* (1), 1603276.
(20) Wang, Q.; O'Hare, D. Recent Advances in the Synthesis and Application of Layered Double Hydroxide (LDH) Nanosheets. *Chem. Rev.* **2012**, *112* (7), 4124−4155.
(21) Peng, L.; Mei, X.; He, J.; Xu, J.; Zhang, W.; Liang, R.; Wei, M.; Evans, D. G.; Duan, X. Monolayer Nanosheets with an Extremely High Drug Loading toward Controlled Delivery and Cancer Theranostics. *Adv. Mater.* **2018**, *30* (16), 1707389.
(22) Li, L.; Gu, W.; Liu, J.; Yan, S.; Xu, Z. P. Amine-Functionalized SiO_2 Nanodot-Coated Layered Double Hydroxide Nanocomposites for Enhanced Gene Delivery. *Nano Res.* **2015**, *8* (2), 682−694.
(23) Vallet-Regi, M.; Ramila, A.; del Real, R. P.; Perez-Pariente, J. A New Property of MCM-41: Drug Delivery System. *Chem. Mater.* **2001**, *13* (2), 308−311.
(24) Tang, F.; Li, L.; Chen, D. Mesoporous Silica Nanoparticles: Synthesis, Biocompatibility and Drug Delivery. *Adv. Mater.* **2012**, *24* (12), 1504−1534.
(25) Li, Z.; Barnes, J. C.; Bosoy, A.; Stoddart, J. F.; Zink, J. I. Mesoporous Silica Nanoparticles in Biomedical Applications. *Chem. Soc. Rev.* **2012**, *41* (7), 2590−2605.
(26) Harrison, R.; Li, L.; Gu, Z.; Xu, Z. P. Controlling Mesoporous Silica-Coating of Layered Double Hydroxide Nanoparticles for Drug Control Release. *Microporous Mesoporous Mater.* **2017**, *238*, 97−104.
(27) Li, P.; Yu, Y.; Huang, P.-P.; Liu, H.; Cao, C.-Y.; Song, W.-G. Core-shell Structured MgAl-LDO@Al-MS Hexagonal Nanocomposite: an All Inorganic Acid-Base Bifunctional Nanoreactor for One-pot Cascade Reactions. *J. Mater. Chem. A* **2014**, *2* (2), 339−344.
(28) Liu, J.; Harrison, R.; Zhou, J. Z.; Liu, T. T.; Yu, C.; Lu, G. Q.; Qiao, S. Z.; Xu, Z. P. Synthesis of Nanorattles with Layered Double Hydroxide Core and Mesoporous Silica Shell as Delivery Vehicles. *J. Mater. Chem.* **2011**, *21* (29), 10641−10644.
(29) Bao, H.; Yang, J.; Huang, Y.; Xu, Z. P.; Hao, N.; Wu, Z.; Lu, G. Q.; Zhao, D. Synthesis of Well-dispersed Layered Double Hydroxide Core@Ordered Mesoporous Silica Shell Nanostructure (LDH@$mSiO_2$) and Its Application in Drug Delivery. *Nanoscale* **2011**, *3* (10), 4069−4073.
(30) Yu, L.; Chen, Y.; Wu, M.; Cai, X.; Yao, H.; Zhang, L.; Chen, H.; Shi, J. "Manganese Extraction" Strategy Enables Tumor-Sensitive Biodegradability and Theranostics of Nanoparticles. *J. Am. Chem. Soc.* **2016**, *138* (31), 9881−9894.
(31) Esatbeyoglu, T.; Huebbe, P.; Ernst, I. M. A.; Chin, D.; Wagner, A. E.; Rimbach, G. Curcumin From Molecule to Biological Function. *Angew. Chem., Int. Ed.* **2012**, *51* (22), 5308−5332.
(32) Ali, S.; Ahmad, A.; Banerjee, S.; Padhye, S.; Dominiak, K.; Schaffert, J. M.; Wang, Z.; Philip, P. A.; Sarkar, F. H. Gemcitabine Sensitivity Can Be Induced in Pancreatic Cancer Cells through Modulation of miR-200 and miR-21 Expression by Curcumin or Its Analogue CDF. *Cancer Res.* **2010**, *70* (9), 3606−3617.
(33) Sun, D.; Zhuang, X.; Xiang, X.; Liu, Y.; Zhang, S.; Liu, C.; Barnes, S.; Grizzle, W.; Miller, D.; Zhang, H.-G. A Novel Nanoparticle Drug Delivery System: The Anti-inflammatory Activity of Curcumin Is Enhanced When Encapsulated in Exosomes. *Mol. Ther.* **2010**, *18* (9), 1606−1614.
(34) Lim, G. P.; Chu, T.; Yang, F. S.; Beech, W.; Frautschy, S. A.; Cole, G. M. The Curry Spice Curcumin Reduces Oxidative Damage and Amyloid Pathology in an Alzheimer Transgenic Mouse. *J. Neurosci.* **2001**, *21* (21), 8370−8377.
(35) Lelli, D.; Sahebkar, A.; Johnston, T. P.; Pedone, C. Curcumin Use in Pulmonary Diseases: State of the Art and Future Perspectives. *Pharmacol. Res.* **2017**, *115*, 133−148.
(36) Padmanaban, G.; Nagaraj, V. A. Curcumin May Defy Medicinal Chemists. *ACS Med. Chem. Lett.* **2017**, *8* (3), 274−274.
(37) Nelson, K. M.; Dahlin, J. L.; Bisson, J.; Graham, J.; Pauli, G. F.; Walters, M. A. Curcumin May (Not) Defy Science. *ACS Med. Chem. Lett.* **2017**, *8* (5), 467−470.
(38) Nelson, K. M.; Dahlin, J. L.; Bisson, J.; Graham, J.; Pauli, G. F.; Walters, M. A. The Essential Medicinal Chemistry of Curcumin. *J. Med. Chem.* **2017**, *60* (5), 1620−1637.
(39) Kocaadam, B.; Sanlier, N. Curcumin, An Active Component of Turmeric (Curcuma Longa), and Its Effects on Health. *Crit. Rev. Food Sci. Nutr.* **2017**, *57* (13), 2889−2895.
(40) Kunnumakkara, A. B.; Bordoloi, D.; Padmavathi, G.; Monisha, J.; Roy, N. K.; Prasad, S.; Aggarwal, B. B. Curcumin, the Golden Nutraceutical: Multitargeting for Multiple Chronic Diseases. *Br. J. Pharmacol.* **2017**, *174* (11), 1325−1348.
(41) Jin, D.; Park, K.-W.; Lee, J. H.; Song, K.; Kim, J.-G.; Seo, M. L.; Jung, J. H. The Selective Immobilization of Curcumin onto the Internal Surface of Mesoporous Hollow Silica Particles by Covalent Bonding and Its Controlled Release. *J. Mater. Chem.* **2011**, *21* (11), 3641−3645.
(42) Gou, M.; Men, K.; Shi, H.; Xiang, M.; Zhang, J.; Song, J.; Long, J.; Wan, Y.; Luo, F.; Zhao, X.; Qian, Z. Curcumin-Loaded Biodegradable Polymeric Micelles for Colon Cancer Therapy. *Nanoscale* **2011**, *3* (4), 1558−1567.
(43) Sintov, A. C. Transdermal Delivery of Curcumin via Microemulsion. *Int. J. Pharm.* **2015**, *481* (1−2), 97−103.
(44) Liu, J.; Chen, Z.; Wang, J.; Li, R.; Li, T.; Chang, M.; Yan, F.; Wang, Y. Encapsulation of Curcumin Nanoparticles with MMP9-Responsive and Thermos-Sensitive Hydrogel Improves Diabetic Wound Healing. *ACS Appl. Mater. Interfaces* **2018**, *10* (19), 16315−16326.
(45) Prevot, V.; Casal, B.; Ruiz-Hitzky, E. Intracrystalline Alkylation of Benzoate Ions into Layered Double Hydroxides. *J. Mater. Chem.* **2001**, *11* (2), 554−560.
(46) Zhao, X.-Z.; Jiang, T.; Wang, L.; Yang, H.; Zhang, S.; Zhou, P. Interaction of Curcumin with Zn(II) and Cu(II) Ions Based on Experiment and Theoretical Calculation. *J. Mol. Struct.* **2010**, *984* (1−3), 316−325.
(47) John, V. D.; Krishnankutty, K. Antitumour Activity of Synthetic Curcuminoid Analogues (1,7-diaryl-1,6-heptadiene-3,5-diones) and Their Copper Complexes. *Appl. Organomet. Chem.* **2006**, *20* (8), 477−482.

DOI: 10.1021/acsabm.8b00343
ACS Appl. Bio Mater. 2018, 1, 928−935

(48) Yoon, H.; Liu, R. H. Effect of Selected Phytochemicals and Apple Extracts on NF-kappa B Activation in Human Breast Cancer MCF-7 Cells. *J. Agric. Food Chem.* **2007**, *55* (8), 3167−3173.

DOI: 10.1021/acsabm.8b00343
ACS Appl. Bio Mater. 2018, 1, 928−935